High-Performance Inertial Measurements Using a Redundant Array of Inexpensive Gyroscopes (RAIG)

John Wang and Edwin Olson

***Abstract*— Orientation estimates derived from gyroscopes are limited in quality by the noise and bias characteristics of the sensors. Presently, there is a large gap in price and performance between high-end fiber-optic gyroscopes and inexpensive MEMS gyroscopes. In this paper, we propose using a redundant array of inexpensive gyroscopes (RAIG) in order to obtain significant improvements in performance.**

A naïve analysis predicts that n gyros should reduce angular rate measurement noise by a factor of $\sqrt{n}$. In this paper, we describe our custom array of 72 gyros which we use to evaluate the empirical scaling performance. This evaluation includes comparisons between several standard filtering and bias estimation algorithms. In addition, we propose a principled algorithm that exploits non-linear dynamics, significantly improving performance.

I. Introduction

The advent of mass-produced microelectrical mechanical systems (MEMS) gyroscopes has enabled ubiquitous motion sensing in cellular phones and other consumer devices. Their low cost and popularity can be attributed to consumer demand and advances in manufacturing technology, which have driven the price of sensors below $10. Today's MEMS sensors are highly integrated, and it is common to find three-axis accelerometers and gyros on the same chip in compact surface-mount packages. The gyroscope and accelerometer combination is commonly referred to as an inertial measurement unit (IMU).

MEMS IMUs are commonly used in robotics applications. In aerial robotics, their small size and light weight are a significant advantage, and even in ground robots, MEMS sensors are often used as they provide adequate performance at a low cost. MEMS IMUs are typically used in conjunction with other sensors that measure translational motion to dead-reckon the robot's position and orientation in the absence of external references.

This dead-reckoned orientation estimate is critical for a robot's higher-level systems such as simultaneous localization and mapping (SLAM). In one common approach to SLAM, the robot's trajectory is formulated as a pose graph optimization problem with constraints coming from both inertial estimates and external landmarks. The inertial estimate accumulates error over distance: a heading error of 1° results in 1 meter of displacement error over 60 meters. Furthermore, this optimization problem is nonlinear due to uncertainty in the robot's orientation, introducing multiple local minima. Therefore, even small improvements in the robot's orientation estimate can have a large effect on the accuracy of the robot's final pose graph.

The authors are with the Computer Science and Engineering Department, University of Michigan, Ann Arbor, MI 48109, USA. {jnwang,ebolson}@umich.edu; http://april.eecs.umich.edu

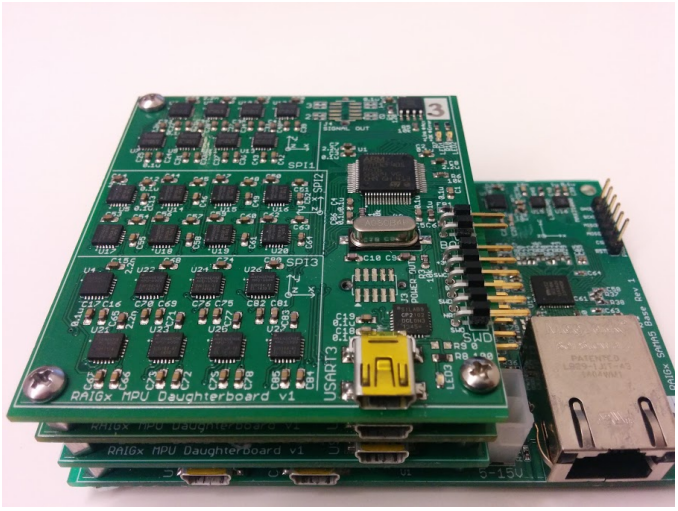

Fig. 1: Our multi-gyro test array. Readings from an array of IMUs can be fused to create a higher-accuracy orientation estimate. Our testbed features 72 Invensense MPU-6000 IMUs stacked in three layers.

Improvements in manufacturing have driven down the cost of consumer-grade MEMS gyros [1]. On the other end of the cost spectrum are high-performance gyros such as fiber-optic gyros, but a gyro that costs thousands of dollars per axis may not make sense for certain robotics applications. While robot localization systems would benefit from more accurate gyroscopes, there is a middle ground of sensor cost and performance with few options. We propose a method that takes advantage of the availability of low-cost MEMS gyros. By fusing the readings of multiple gyros, the quality of our orientation estimates can be improved. The chief contributions of this work are:

- An empirical analysis of performance scaling with multiple identical gyros, showing the practical limit of existing multi-gyro approaches
- A multi-gyro fusion algorithm incorporating a nonlinear motion model that significantly reduces angular error over existing approaches
- A novel multi-gyro dataset for evaluating filter performance

II. Background and Prior Work

The idea of combining measurements from multiple gyroscopes into a single, higher-accuracy "virtual gyroscope" was first proposed by Bayard and Ploen [2]. Their method uses a Kalman filter to combine gyro readings, which is optimal given their assumptions of a linear system with additive Gaussian white noise. They develop a closed-form analysis of the Ricatti differential equation of the multiple-gyro system, from which come two important theoretical properties. First, with n identical uncorrelated devices, the resulting gyro will have its drift reduced by a factor of $\sqrt{n}$. This corresponds to the theoretical limit of noise reduction by signal averaging, where the average of n signals with independent, uncorrelated noise will yield a $\sqrt{n}$ reduction in noise. In practice, this limit may not be reached due to positively correlated noise. The second result of their paper shows that negatively correlated gyros can improve drift beyond the $\sqrt{n}$ limit. They showed that as the correlation coefficient ρ approaches -1 (perfect negative correlation), the amount of drift approaches zero. With multiple gyros, sufficient negative correlation can result in a drift-free virtual gyro reading. Intuitively, this can be explained as a differential-mode signal between two gyros: if the drift noise is perfectly negatively correlated between two gyros, then averaging the two gyro signals results in a drift-free motion estimate. In this paper we provide empirical answers to complement the results from Bayard and Ploen. We characterize the correlation between low-cost MEMS gyros to determine whether they are favorable or unfavorable to noise reduction.

Methods have been proposed to deal with bias drift by creating the type of negative correlation that results in differential-mode rejection. For gyrocompassing, a demanding application which requires detection of the earth's rotation rate, there are two general approaches, indexing and carouseling [3], [4]. In indexing, a gyro is alternately read at an orientation of 0 and 180 degrees from a fixed position. The readings are subtracted, cancelling out bias drift, since the bias drift happens at timescales much larger than the measurement rate. In carouseling, the gyro is continuously rotated and sampled at a fast enough rate that gyro biases are integrated out with every complete revolution. While both methods produce a drift-free bias reading, they have the disadvantage of requiring actuation. In our work, we focus entirely on non-actuated approaches.

With angular rate gyros, orientation is determined by integrating a noisy rate signal. As the rate drifts, there are two components of noise both modeled as white noise processes by Bayard and Ploen. The gyro output $z(t)$ is a combination of the angular rate $\omega(t)$, a bias of $b(t)$, and zero-mean white noise $v(t)$. The bias is assumed to follow a random walk, so it is the integral of zero-mean white noise $w(t)$.

$$z(t) = \omega(t) + b(t) + v(t) \tag{1}$$

$$\dot{b}(t) = w(t) \tag{2}$$

We will use a generalization of the same basic formulation where the noise processes can be arbitrarily complex. The two components of noise are the angular random walk caused by $v(t)$ and rate random walk caused by $w(t)$. Angular random walk has units of $\deg/s^{1/2}$, meaning that it contributes to orientation error at a sublinear rate with respect to time. Rate random walk, which is sometimes called bias drift, has units of $\deg/s^{3/2}$. As the rate error is integrated into the orientation, it causes orientation error to accumulate superlinearly with respect to time. It is important to note that both angular random walk and rate random walk can cause unbounded orientation error. However, the rate random walk is the primary contributor to orientation error over long integration periods for typical MEMS devices.

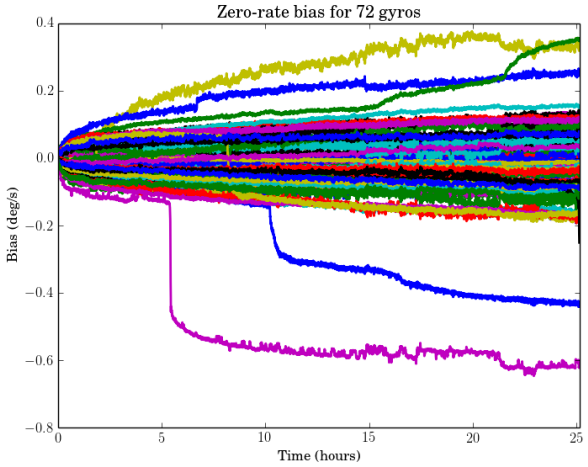

Fig. 2: Zero-rate bias of 72 gyros observed over 25 hours. Most gyro biases follow the distribution of a random walk, where the standard deviation grows proportionally to the square root of time. Some outlier gyros (e.g. in purple and blue) experience large jumps in bias not described by the random walk model.

A common approach to dealing with rate random walk is to integrate readings over shorter time periods. This method involves a zero-velocity detector based on the known dynamics of the system. Instead of integrating error at a superlinear rate over time, the zero-velocity update breaks the chain of observations into smaller timescales where the bias can be considered constant. Automatic zero-velocity updates may be achieved by analyzing the variance of the gyroscope signal [5]. One application of zero-velocity detection is in IMU-based pedestrian tracking [6], [7], where the accelerometer and gyro biases are updated every time the foot hits the ground. Heuristic methods can be employed in vehicle tracking, assuming that motion commonly occurs in a straight line [8]. If motion is detected in a straight line, the system can explicitly remove gyro bias error from orientation estimates. However, in both these cases, the zero-velocity or straight-line detectors must be explicitly defined and tuned for the particulars of the system. In our work, we will present an alternative method that reduces drift due to bias changes without computing explicit bias updates.

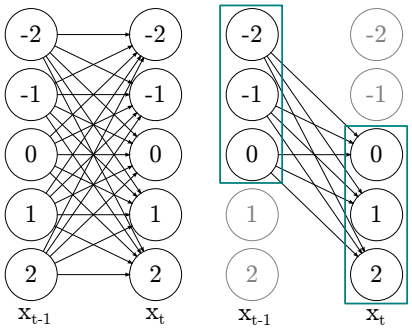

Fig. 3: Illustration of windowing to reduce state space dimensionality. The full state space is shown on the left, and the windowed state space on the right. For each timestep only a subset of states are active, and other states are ignored. This effectively assumes they have zero probability.

III. Proposed Method

Our proposed method poses the gyro filtering problem as a hidden Markov model (HMM). The hidden variables x_t are the true angular rate over time, while the observation vector z_t is corrupted with noise and biases for each observation. The forward algorithm efficiently computes the posterior distribution $P(x_t|z_{1:t})$ over the current state given the sequence of observations $z_{1:t}$ [9]. By the Markov property, x_{t+1} is conditionally independent of $x_{1:t-1}$ given the current state x_t. Therefore we can recursively update the probability distribution at each timestep, marginalizing out the previous state:

$$P(x_{t+1}|z_{1:t+1}) = P(z_{t+1}|x_{t+1}) \sum_{x_t} P(x_t|z_{1:t}) P(x_{t+1}|x_t)$$

$P(z_{t+1}|x_{t+1})$ is the emission or observation probability, $P(x_{t+1}|x_t)$ is the transition probability derived from the motion model, and $P(x_t|z_{1:t})$ is the posterior at the previous timestep. We can recover the maximum likelihood estimate by taking:

$$\hat{x}_t = \arg\max_{x_t} P(x_t|z_{0:t})$$

In order to use the forward algorithm on our HMM, we discretize the state space of possible angular rates. It should be noted that although angular velocity is a continuous variable, the gyro readings themselves are already discrete integer values. To reduce quantization error, the state space is discretized at a resolution of $\frac{1}{512}^\circ/s$ per LSB, which effectively provides 3 bits of increased resolution compared to the raw 16-bit readings from our gyros.

The computation time of the forward algorithm grows with the square of the number of states. As it is impractical to store and compute updates for 2^{19} states, we propose an approximate filtering method. Instead of computing updates for all 2^{19} states at each timestep, we treat only a window of 128 states as active for each timestep (illustrated in Figure 3). The center of this window is determined at each timestep by a crude pre-filter which only needs to estimate the angular velocity within $\pm\frac{1}{8}^\circ/s$, which is easily achieved with current methods. This window can be enlarged at the cost of additional computation time. For our prefilter estimate we take the average of all our gyro readings at a single timestep.

A. Noise model

The angle random walk is modeled as additive Gaussian white noise with standard deviation σ_n. In a noise-only model the probability of an observation z_t is as follows:

$$P(z_t|x_t) \propto \exp\left(-\frac{(z_t - x_t)^2}{2\sigma_n^2}\right)$$

B. Bias model

An advantage of our formulation is that the biases of each gyro are not explicitly estimated. Instead, the bias for each gyro i is implicitly determined by the filtered angular rate estimate by equation (1): $b_i(t) = z_i(t) - \omega(t)$. This keeps the size of the state space constant as the number of gyros increases, which is important for large arrays of gyros.

Although the bias is not included in the state vector, we can still model the bias in our formulation. An additional term is added to our observation model, penalizing choices of ω that cause large changes in bias. First, the bias estimates of each gyro are filtered to remove angle random walk noise. Then the derivative of the bias $\dot{b}(t)$ is estimated numerically. In our implementation, bias is modeled as a Gaussian random walk with σ_b. In principle, non-Gaussian distributions for $\dot{b}(t)$ can be handled by our formulation. The observation model gains an additional bias term, corresponding to our model for the rate random walk:

$$P(z_t|x_t) \propto \exp\left(-\frac{(z_t - x_t - b_{t-1})^2}{2\sigma_n^2}\right) \exp\left(-\frac{\dot{b}_t^2}{2\sigma_b^2}\right)$$

C. Motion model

The primary advantage of using the forward algorithm to estimate the hidden state is the ability to use a nonlinear system model. In this discrete-time HMM, the system motion model is encoded in the transition probability $P(x_t|x_{t-1})$.

With an uninformative motion model, bias drift is unobservable since it is indistinguishable from the actual angular rate signal. The motion model allows the filter to assign greater probability to either interpretation of the signal: whether it is drift or true motion. Intuitively, this is similar to the heuristic-based approach in previous work, where knowledge that the vehicle often stops is used to explicitly estimate the bias. In our formulation, the motion model generalizes this concept and removes the need for explicit estimation of the stopped condition. Any model of the system's motion can be plugged in to improve filter performance. Since the motion model is dependent on the system, there is no general prescription for what to use. In the results, we will show two examples of motion models that we used: a simple motion model inspired by the zero-velocity update and a learned motion model based on actual motion data.

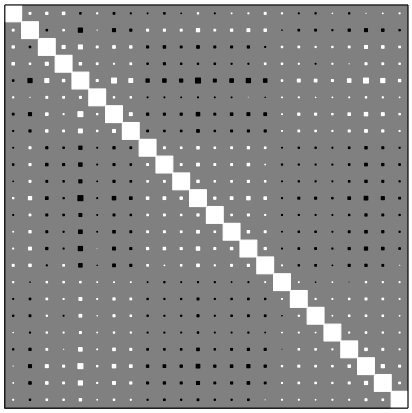

Fig. 4: Correlation between 24 gyros. Black is negative and white is positive. The block structure reflects the physical layout of the gyros, where gyros 9-16 are mounted at a 90 degree rotation from gyros 1-8 and 17-24. Although absolute values vary across runs, the signs of the values forming the block structure are present across runs.

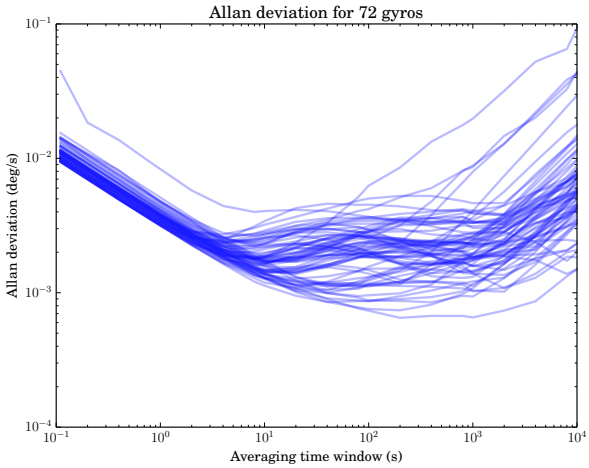

Fig. 5: Allan variance plot for 72 individual gyros. Some salient features can be observed: the value at $\tau = 1$ second indicates an average angle random walk of $0.23^\circ/\sqrt{hr}$, and the minimum value which defines bias stability occurs between 10 and 100 seconds.

IV. Evaluation

A. Description of gyro testbed

To test our method, we designed and fabricated a testbed with 72 Invensense MPU-6000 IMUs, each containing a 3-axis gyroscope, 3-axis accelerometer, and temperature sensor (Figure 1). Designed to test gyro scaling performance, the platform is composed of three stacking boards of 24 IMUs each, with the capacity to add additional boards as needed. The Invensense chip contains internal ADCs for each sensor channel, producing a digital output with 16 bits of resolution. The gyro data is read at 1kHz (their maximum output rate) and integrated by the onboard microcontroller. The integrated measurements are then logged at 100Hz.

For the sake of our intended robotics application, we focused on z-axis (yaw) gyro performance. The roll and pitch angles of a robot can be independently observed by using the onboard accelerometers to observe the gravity vector, but the yaw angle is not observable in an independent manner by onboard sensors. However, the proposed approach would naturally extend to pitch and roll.

B. Correlation

In [2] it was shown that significant negative correlations between gyros in an array can reduce drift by orders of magnitude beyond the expected $\sqrt{n}$ factor improvement. To characterize the limits of our system performance, we analyzed the correlation between our gyros. The analysis over a single board of 24 IMUs shows that the z-axis gyros correlated in a block pattern, as shown in Figure 4. The middle eight gyros are negatively correlated with the first and last eight. This may arise from the physical layout of the board, as the middle block of eight gyros are rotated 90 degrees in the z axis with respect to the first and last block. The gyros that are facing the same way are slightly positively correlated. However, the magnitudes of both positive and negative correlations are very small.

C. Allan variance

To determine the noise performance of our n-gyro array, we measured its Allan variance [10], a widely-accepted statistical method to characterize the noise of a gyro [11]. Allan variance expresses the variance of a signal as a function of the time window over which the signal is averaged. Over small timescales, the angle random walk dominates the noise. As the averaging time window increases, variance decreases due to reduction of angle random walk noise. This trend does not continue indefinitely as the window increases, since variance begins increasing due to the effects of rate random walk. The minimum value of Allan variance at this inflection point is commonly referred to as the bias stability of a gyro. It may be seen as an optimistic lower bound on how quickly angular error accumulates, assuming the longest possible averaging window. (This averaging window may be impractical, as it also filters out the dynamics of the system.) The value on the x-axis is the time window which minimizes the variance of the signal, and is used as the averaging period for initial bias calibration. Beyond this point, the rate random walk's superlinear-growing error overtakes the angle random walk's sublinear-growing error.

The Allan deviation (square root of Allan variance) of the z-axis gyro of each of our 72 IMUs are plotted in Figure 5. The angle random walk is the value of the Allan deviation at $\tau = 1$ second, representing the standard deviation of the angle in degrees per square root second. The average angle random walk of these gyros was $0.23^\circ/\sqrt{hr}$, and the bias stability was $5.8^\circ/hr$. A virtual gyro formed by

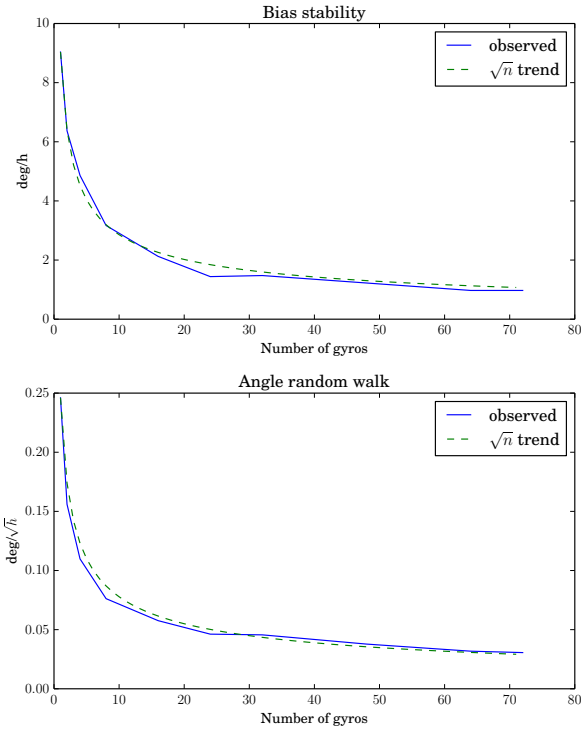

Fig. 6: Bias stability and angle random walk reduction from averaging n gyros. The performance seems to track the theoretical $\sqrt{n}$ decrease in noise and bias stability for uncorrelated gyros.

simple averaging of n gyros matched the predicted $\sqrt{n}$ decrease in noise (Figure 6), supporting our analysis that these gyros are not strongly correlated either positively or negatively. Also, our experimental results show that with near-uncorrelated gyros, simple averaging performs about as well as the Kalman filter described in [2].

D. Results under controlled motion

We evaluate the performance of our system using data collected from a servo-actuated platform. Our 72-gyro testbed is mounted on a platform actuated in the yaw direction by a Dynamixel digital servo, and the servo feedback is logged as ground truth for evaluation[1]. The gyros are rotated back and forth 180 degrees at an angular velocity selected uniformly at random. The platform speeds up with constant acceleration to its target angular velocity, and is decelerated at its goal position as quickly as possible. The motion histogram (Figure 7) shows the pattern of constant acceleration and rapid deceleration.

We implemented two motion models for this system, based on the controlled motion of the servo-driven test platform. The first is a learned motion model which is trained from the servo ground truth of a separate training set. The motion histogram used as the motion model (Figure 7) was regularized with a Gaussian kernel around each sample point. The

[1]Our full test data is available online at `http://april.eecs.umich.edu/raig/`

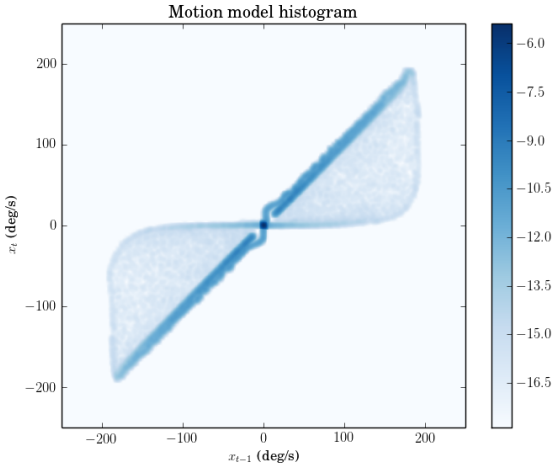

Fig. 7: Motion histogram of the controlled motion test. The histogram shows the transition matrix as $\log P(x_t|x_{t-1})$, the log probability that the angular velocity is x_t given that the previous angular velocity was x_{t-1}. This motion model was generated using the servo feedback as ground truth.

second is a simple motion model that encodes that the system is more likely to be still than moving, with a probability peak at zero velocity and uniform probability elsewhere. (γ is the normalization factor that makes the probabilities sum to 1.)

$$P(x_t|x_{t-1}) = \begin{cases} 10/\gamma & \text{if } x_t = 0 \text{ and } x_{t-1} = 0 \\ 1/\gamma & \text{otherwise} \end{cases}$$

The system is evaluated by computing the average magnitude of yaw error accumulated over integration periods of 10 minutes and 1 hour, respectively. Figures 8 and 9 show results from one of three collected datasets (all three of which are available online). The average error across a large number of runs is shown with respect to the number of gyros used. We implemented two baseline methods: the Kalman filter described in [2], and a mean filter which averages the readings of n gyros at each timestep. According to [2] the reduction in drift should be a factor of $\sqrt{n}$ for n uncorrelated gyros. However, we see that the scaling of performance with n tails off more sharply than the theory would predict, and final error does not improve significantly beyond $n = 10$ gyros. This is likely due to the presence of correlated noise in the long-term bias. One major source of unmodeled correlated noise is temperature, since the zero-rate bias is known to exhibit temperature sensitivity.

The results show that our proposed method improves performance significantly over the baseline methods. The Kalman filter is evaluated using three choices of parameters: uncorrelated ($\rho = 0$), negatively correlated ($\rho = -0.01$), and the empirical covariance matrix shown in Figure 4. The Kalman filter variants and mean filter all perform similarly, and using the empirical covariance matrix with the Kalman filter makes no difference over assuming no correlation (Figure 8). The learned motion model does not significantly

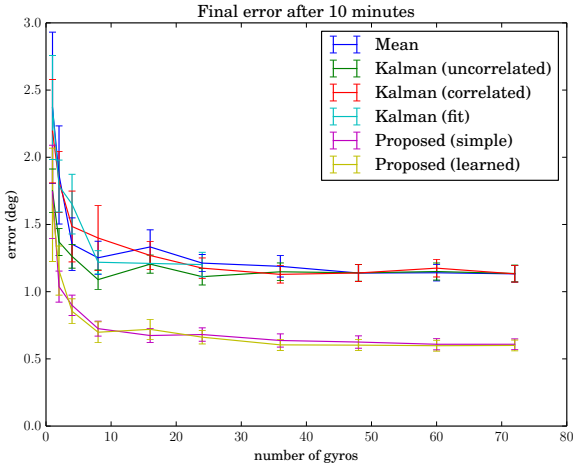

Fig. 8: Average error after 10 minutes over 100 runs. The Kalman filter with uninformative motion model performs similarly to a simple averaging filter. Our proposed method, which allows the use of a nonlinear motion model, results in a 45% reduction in error. There is no measurable performance gain from the learned motion model compared to the simple motion model.

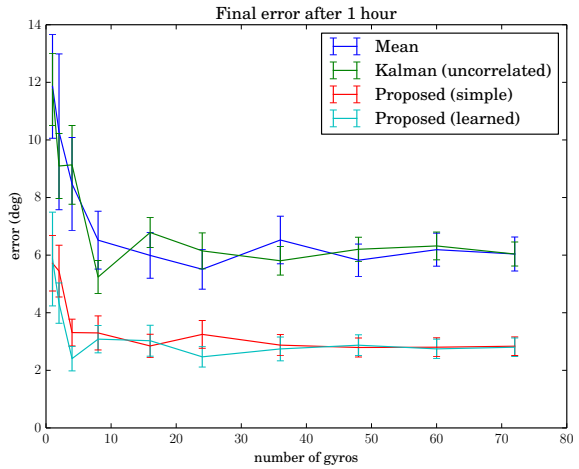

Fig. 9: Average error after 1 hour over 20 runs. Our proposed method reduces the angle error by about 50%.

improve performance over the simple motion model, showing that our method can operate on very general assumptions about the system motion.

V. Conclusion

We presented an empirical analysis of gyro scaling performance using an array of low-cost MEMS gyros. While the noise floor of the gyros does decrease by a factor of $\sqrt{n}$ as predicted, gyros in practice may exhibit long-term bias correlations that limit their scaling performance. We also presented a principled filter incorporating a nonlinear motion model which significantly reduces angular error over existing methods. The motion model is seen as an analog to existing methods (e.g. zero-velocity updates) which compute explicit bias updates, except that bias updates are computed implicitly within the filter. Finally, we present our novel datasets of 72 gyros under controlled motion, which we believe are unique in their scale, to aid future work in multi-gyro synthesis.

Acknowledgments

This work was funded by DARPA Grant D12AP000059.

References

[1] S. Nasiri *et al.*, "A critical review of MEMS gyroscopes technology and commercialization status," *Avaliable online: http://invensense.com/mems/gyro/documents/whitepapers/MEMSGyroComp.pdf*, 2009.

[2] D. S. Bayard and S. R. Ploen, "High accuracy inertial sensors from inexpensive components," Apr. 19 2005, US Patent 6,882,964.

[3] I. P. Prikhodko, S. A. Zotov, A. A. Trusov, and A. M. Shkel, "What is MEMS gyrocompassing? Comparative analysis of maytagging and carouseling," *Microelectromechanical Systems, Journal of*, vol. 22, no. 6, pp. 1257–1266, 2013.

[4] B. M. Renkoski, "The effect of carouseling on MEMS IMU performance for gyrocompassing applications," Ph.D. dissertation, Massachusetts Institute of Technology, 2008.

[5] E. Olson, J. Strom, R. Morton, A. Richardson, P. Ranganathan, R. Goeddel, M. Bulic, J. Crossman, and B. Marinier, "Progress towards multi-robot reconnaissance and the MAGIC 2010 competition," *Journal of Field Robotics*, vol. 29, no. 5, pp. 762–792, September 2012.

[6] E. Foxlin, "Pedestrian tracking with shoe-mounted inertial sensors," *Computer Graphics and Applications, IEEE*, vol. 25, no. 6, pp. 38–46, 2005.

[7] Y. S. Suh and S. Park, "Pedestrian inertial navigation with gait phase detection assisted zero velocity updating," in *Autonomous Robots and Agents, 2009. ICARA 2009. 4th International Conference on*. IEEE, 2009, pp. 336–341.

[8] J. Borenstein and L. Ojeda, "Heuristic reduction of gyro drift in vehicle tracking applications," *International journal of vehicle information and communication systems*, vol. 2, no. 1, pp. 78–98, 2009.

[9] S. J. Russell and P. Norvig, *Artificial Intelligence: A Modern Approach*, 2nd ed. Pearson Education, 2003.

[10] D. W. Allan, "Statistics of atomic frequency standards," *Proceedings of the IEEE*, vol. 54, no. 2, pp. 221–230, 1966.

[11] N. El-Sheimy, H. Hou, and X. Niu, "Analysis and modeling of inertial sensors using allan variance," *Instrumentation and Measurement, IEEE Transactions on*, vol. 57, no. 1, pp. 140–149, 2008.